Wind tunnel investigation of critical flight regimes using dynamically scaled actively controlled model in 3DOF gimbals

I. Grishin, A.Khrabrov, K. Kolinko, .M. Sidoryuk,
Central Aerohydrodynamic Institute (TsAGI)
Zhukovsky, Russia

Abstract

This paper presents a method of studying the critical flight regimes using the three degrees of freedom (3DOF) gimbals in a wind tunnel (WT). The dynamics of a scaled actively controlled model of an aircraft in 3DOF gimbals is considered. Possibility of wind tunnel research of the aircraft dynamics at high angles of attack by means of a scaled model in 3DOF gimbals is justified. Two control algorithms suppressing self-induced large amplitude lateral/directional oscillations (wing rock) and stalling are proposed. The wing rock and stalling prevention is validated using nonlinear time-domain simulations and experimental studies with dynamically scaled controlled model in 3DOF gimbals.

1. Introduction

The dynamics of modern aircraft is complicated via extending the flight envelope. At high angle of attack a set of dangerous phenomena such as development of large-amplitude self-induced oscillations or spin can occur. Large-amplitude roll/yaw oscillations known as wing-rock arise at angles of high angles of attack. They not only limit the maneuverable performance of the aircraft but also can lead to its crashing. Great emphasis has been placed on this problem for many years. Numerous studies have been conducted, with the aim of understanding the mechanism of the appearance of these self-induced oscillations and developing an adequate nonlinear aircraft aerodynamic model.

The study of flight dynamics at high angles of attack requires a mathematical model of unsteady aerodynamic characteristics, which is traditionally developed based on the results of experimental investigations of static and dynamic WT tests using the forced oscillations rigs. The problems of flight dynamics at high angles of attack are highly non-linear due to flow separation development. So it would be interesting and productive to study the dynamics and aerodynamics of the aircraft directly in critical flight modes. From this point of view, it is of great interest to perform the experimental study of the free model oscillations, leading to stalling which are dynamically similar to those observed in flight.

For the experimental approximation of the natural unsteady flight motion of the aircraft it is possible to use three-degree-of-freedom gimbals and actively controlled dynamically scaled aerodynamic model. There were a series of works devoted to designing control laws for actively controlled aircraft models ‘flying’ in multiple degrees of freedom in wind tunnels. Single degree-of-freedom rigs with actuated control surfaces were used for investigation of stability and control by many authors [1-8]. A 2DOF rig (roll and yaw) using active control surfaces augmented with compressed-air blowing was developed and successfully used for testing H_∞ - control laws in [9]. Three and more degree of freedom rigs were developed and used in [10-12] to extract aerodynamic models, develop control systems and perform wind tunnel simulations of dynamic motions.

A full 6 DOF free flight setup was developed by NASA for the large-scale wind tunnel [13]. The tested model is free flying within the tunnel working section, with electrical power, compressed air and control signals from outside controllers and using three operators providing command control inputs on three channels. The cost of this type of setup is very high. A 5 DOF pilot rig was developed and tested for a few degrees of freedom at the University of Bristol [10-11]. In [11] the ventral sting perpendicular to the flow of WT was used. It has been shown that the use of the dynamically scaled controlled model mounted on the three-degrees-of-freedom gimbals in WT allows obtaining an efficient and cost-effective study of aircraft static and dynamic stability derivatives and investigation of stability and control. However, this kinematic scheme allows study of unsteady aerodynamic characteristics only in a limited range of small and medium angles of attack. Limitations of kinematics due to the ventral sting do not allow investigation of the process of stalling, and especially the spin motion.

In the present work the use of the dorsal sting located along the wind tunnel flow velocity is proposed. Thus many of the restrictions associated with the ventral holder can be removed. The proposed 3-DOF rig allows investigation of large angles of attack phenomena, such as longitudinal pitching limit-cycle oscillations, or lateral–directional phenomena, such as wing rock and stalling. The paper present a method of investigation of high angle of attack phenomena using developed in TsAGI experimental tools. The experimental setup allows not only control motion of a scaled aircraft model in 3-DOF gimbals, but conduct also measurement of state and dynamic aerodynamic derivatives or their identification from the records of parameters of the model motion under different step-wise and sinusoidal control inputs. So iterative creating of aerodynamic model and using it to control law design may better describe the controllable dynamics of the aircraft at high angles of attack.

2. Experimental rig

A schematic view of a dynamic rig in WT (sting located along the velocity of the flow) is shown in Figure 1.The aircraft model being used for the wind tunnel rig has wing span about 1m. Its mass is about 4.5 kg. It has a conventional set of control surfaces driven by model aircraft servos. The aircraft model is controlled via a wireless link, which also serves for data transfer. 3-DOF gimbals are used to achieve rotation in three degrees of freedom: pitch, roll, and yaw. Except 3DOF motion, the facility provides any single-DOF configuration and any 2DOF motion combination. The attitude of the model in gimbals is measured by three high resolution optical encoders (accuracy $\pm 0.07^{o}$). An inertial measurement unit supplied by Kalman filter is used also. Angular velocities are measured by gyros placed inside the model with accuracy $\pm 0.025^{o}$/s. Data acquisition is performed at frequency 100Hz, and control is performed at 50Hz using real-time control system. The wind tunnel experiments were performed at flow speed 25 m/s. A wind tunnel flow turbulence level is approximately 3%. Figure 2 gives a view of the measuring unit and on-board computer, as well as 3DOF gimbals. Figure 3 shows a screen view of the managing software.

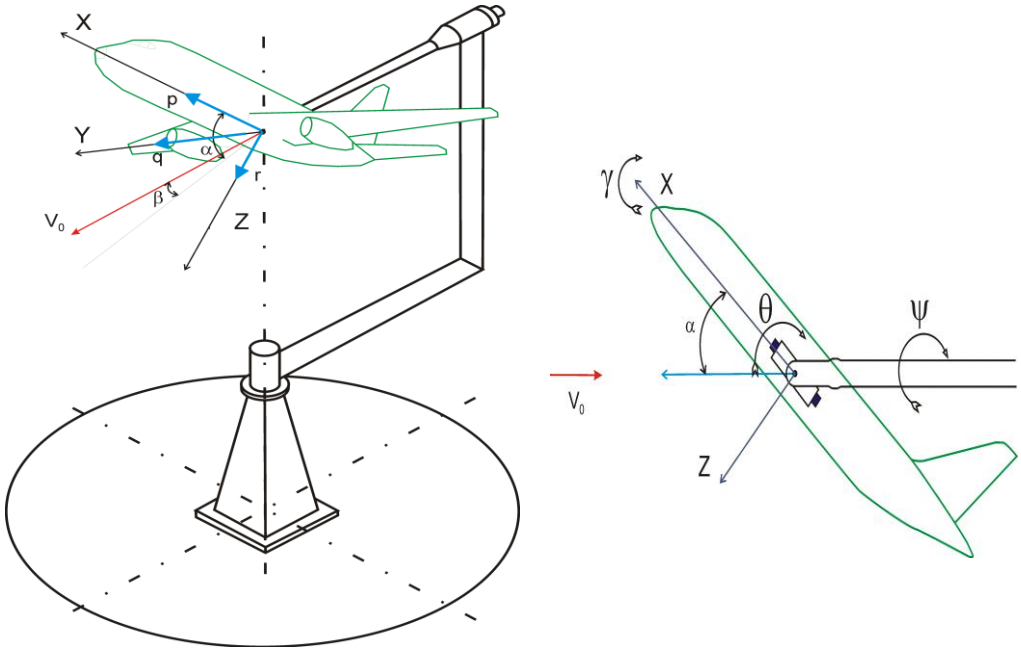

Figure 1: A scheme of three-degree-of-freedom dynamic rig in WT

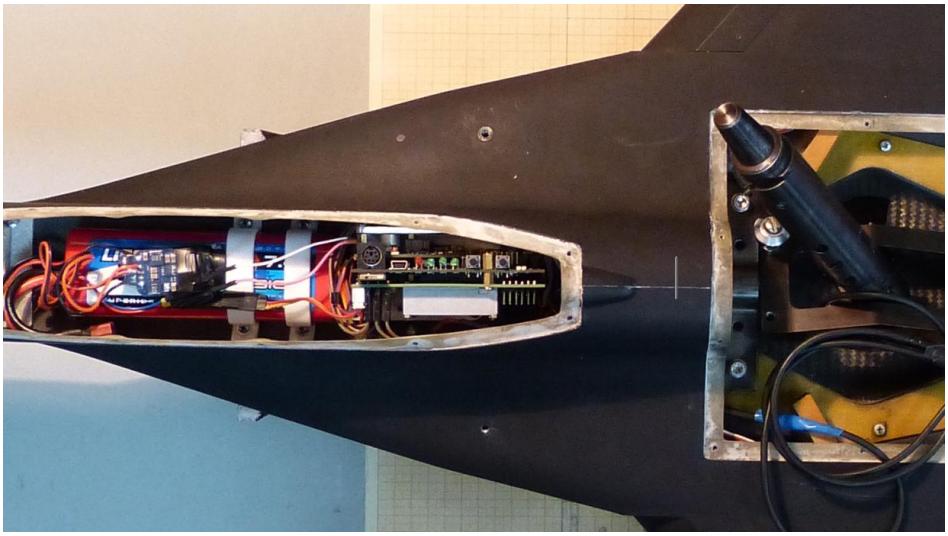

Figure 2: Measurement unit with on-board computer, and 3DOF gimbals

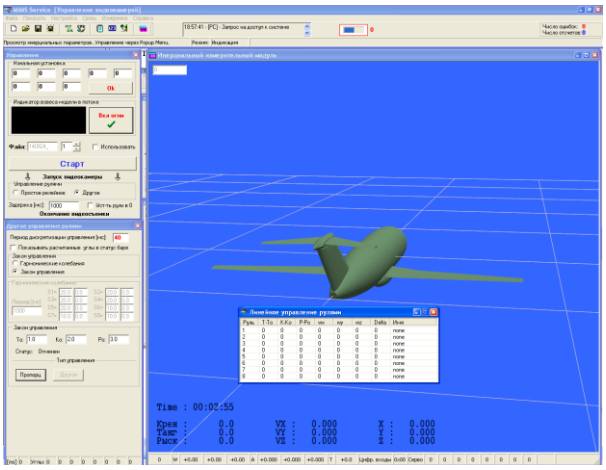

Figure 3: Software for experiment management

3. Mathematical model of a controlled model in 3 DOF gimbals

Position of the aircraft model in the 3DOF gimbals is defined by three Euler angles ψ, θ, γ (Figure 1)/. Yaw angle ψ lies in the range [-180, 180] degrees. The dorsal holder allows pitch angle θ vary inside the interval [20, 120] degrees, and roll angle vary in the range [-40, 40] degrees. The dynamics of the aircraft model in the 3DOF gimbals is described by the following system of differential equations [14-15]:

$$\begin{aligned} \dot{\theta} &= -r\sin\gamma + q\cos\gamma, \\ \dot{\psi} &= (r\cos\gamma + q\sin\gamma)/\sin\theta \\ \dot{\gamma} &= p - (r\cos\gamma + q\sin\gamma)/\tan\theta \\ \dot{\omega} &= J^{-1}(-\omega \times J\omega + M_a(\alpha,\beta,\omega,\delta) + M_g + M_f) \end{aligned} \tag{1}$$

where $\omega=(p,q,r)^T$ is a vector of body-axis angular velocity components of the model, $\delta = (\delta_e, \Delta\delta_e, \delta_a, \delta_r)^T$ is a control vector consisting on elevator δ_e,, differential elevator $\Delta\delta_e$,, aileron δ_a, and rudder surface δ_r deflections. M_a, M_g, and M_f are aerodynamic, gravity, and gimbals friction forces moments, respectively. Angle of attack α and sideslip angle β are defined by the following relations:

$$tg\alpha = tg\theta\cos\gamma,$$
$$\sin\beta = \sin\theta\sin\gamma.$$

Body-axis components of non-dimensional aerodynamic moment have the following form:

$$\begin{aligned} C_m &= C_{m0}(\alpha,\delta_e) + C_{mq}(\alpha)q \\ C_l &= C_{l\beta}(\alpha,\beta) + C_{lp}(\alpha)p + C_{lr}(\alpha)r + C_{l\delta_a}(\alpha,\delta_a) + C_{l\delta_r}(\alpha,\delta_r) + \Delta C_l(\alpha,\delta_e,\Delta\delta_e) \\ C_n &= C_{n\beta}(\alpha,\beta) + C_{np}(\alpha)p + C_{nr}(\alpha)r + C_{n\delta_a}(\alpha,\delta_a) + C_{n\delta_r}(\alpha,\delta_e,\delta_r) + \Delta C_n(\alpha,\delta_e,\Delta\delta_e) \end{aligned} \quad (2)$$

where nonlinear dependences $C_i(\alpha, \beta, \delta)$ (i = l ,m, n) are obtained from the results of experimental investigations of static and dynamic tests in wind tunnel using the forced oscillations rigs in pitch, roll and yaw. Some of these nonlinear dependences for the considered aircraft model are presented in Figures 2-4. The dependence of non-dimensional roll and yaw moments on sideslip angle and angle of attack are presented in Figure 2, while the dependence of these moments on angle of attack and rudder deflections are shown in Figure 3, and from aileron deflections in Figure 4. It can be seen that the presented aerodynamic characteristics are highly nonlinear, and control efficiency strongly decreases at high angles of attack.

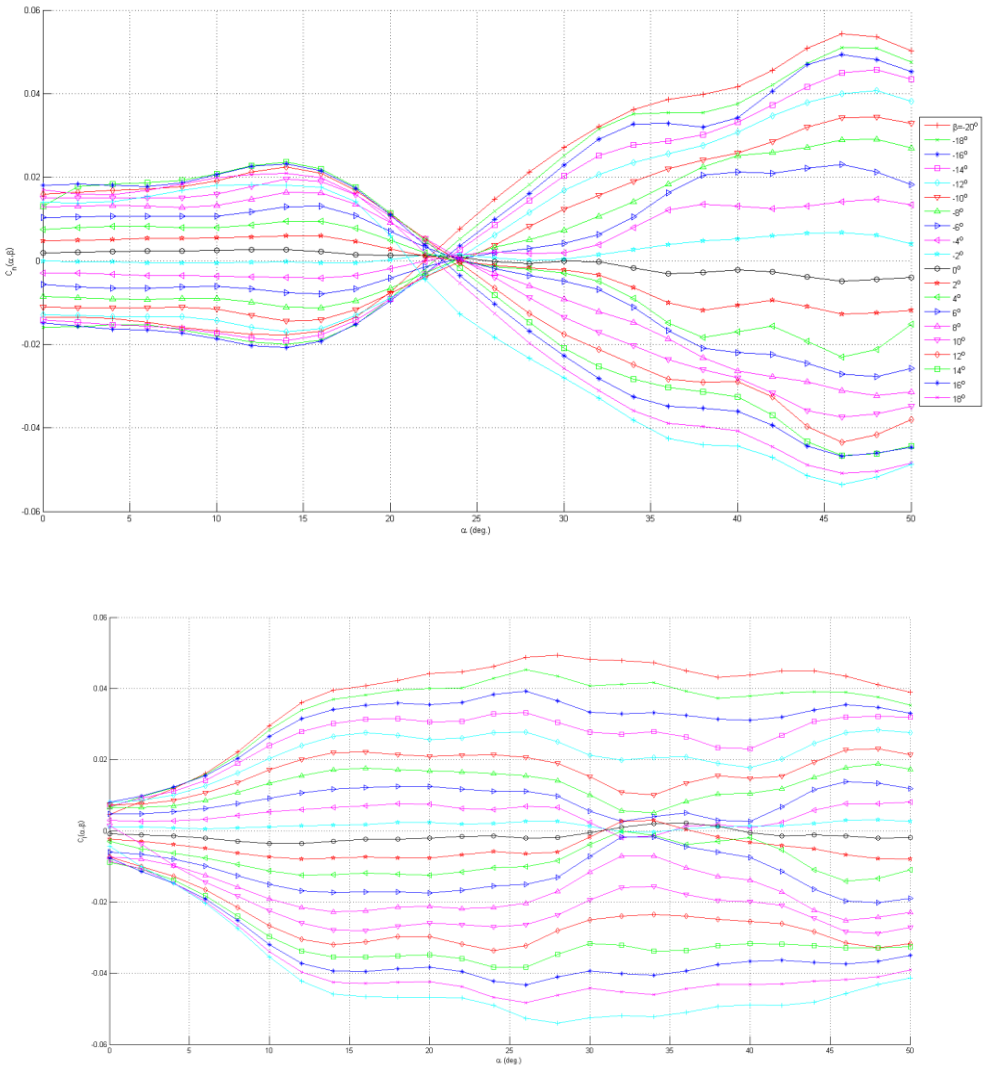

Figure 4: Dependence of non-dimensional roll and yaw moments on sideslip angle and angle of attack.

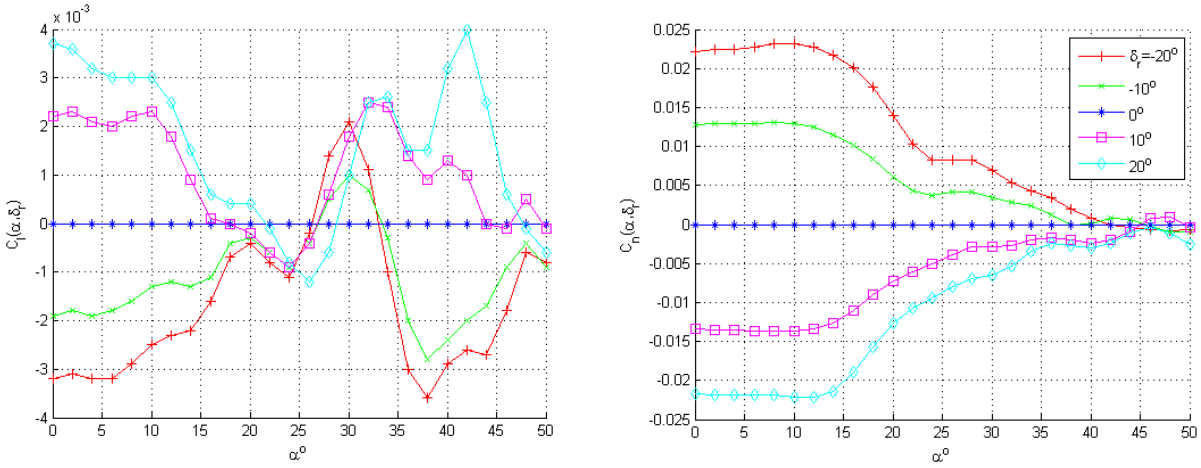

Figure 5: Dependence of non-dimensional roll and yaw moments on sideslip angle and rudder deflection.

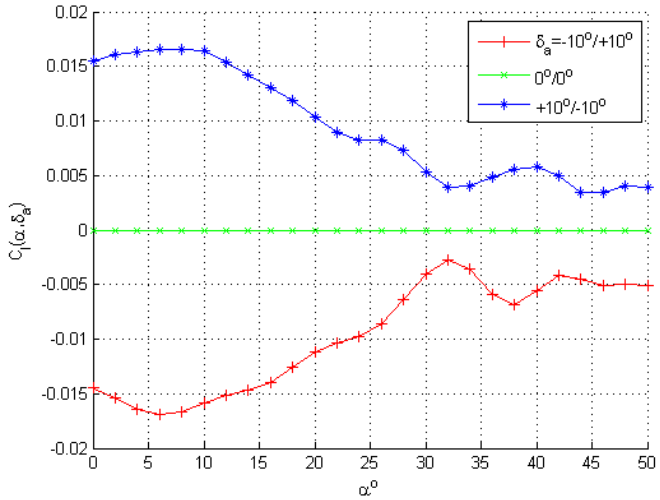

Figure 6: Dependence of non-dimensional roll moment on angle of attack and aileron deflection.

Gravity forces moment M_g in equations (1) due to the inability to accurately match the center of mass and the center of the gimbals center. Body-axis components M_{gx}, M_{gy}, M_{gz} of gravity moment M_g are the following (the displacement of the center of mass along y-axis is neglected):

$$M_{gx} = mg\Delta z_{c.g.}(\sin\psi\cos\gamma + \cos\psi\cos\theta\sin\gamma)$$
$$M_{gy} = -mg\Delta x_{c.g.}\cos\psi\cos\theta\cos\gamma + mg\Delta z_{c.g.}\cos\psi\sin\theta$$
$$M_{gz} = mg\Delta x_{c.g.}(\sin\psi\cos\gamma + \cos\psi\cos\theta\sin\gamma).$$

Friction moment in each axis of rotation (ψ,θ,γ) is modeled as a sum of dry and viscous friction with some coefficients to be identified:

$$Q_{f\psi} = -k_{1\psi}\operatorname{sign}\dot{\psi} - k_{2\psi}\dot{\psi}, \quad Q_{f\theta} = -k_{1\theta}\operatorname{sign}\dot{\theta} - k_{2\theta}\dot{\theta}, \quad Q_{f\gamma} = -k_{1\gamma}\operatorname{sign}\dot{\gamma} - k_{2\gamma}\dot{\gamma}.$$

Body-axis components M_{fx}, M_{fy}, M_{fz} of friction moment M_f are as follows:

$$M_{fx} = Q_{f\gamma}$$
$$M_{fy} = Q_{f\theta}\cos\gamma - (Q_{f\gamma}\cos\theta - Q_{f\psi})\sin\gamma/\sin\theta$$
$$M_{fz} = -Q_{f\theta}\sin\gamma\text{-}(Q_{f\gamma}\cos\theta - Q_{f\psi})\cos\gamma/\sin\theta.$$

To identify the coefficients of dry $k_{1\theta}$, $k_{1\gamma}$, $k_{1\psi}$ and viscous $k_{2\theta}$, $k_{2\gamma}$, $k_{2\psi}$ friction and displacement of the center of gravity relative to the center of the gimbals, special experiments were performed. Free oscillations of the aircraft model without flow for each of the axis of gimbals, as well as oscillations on a spring suspension were recorded. Approximation of the experimental records and numerical simulation results of the corresponding motions with the same initial conditions were compared, minimizing one of the following target functions:

$$F_i = \left\| \theta_{exper}(t) - \theta_{simul}(t, k_{1i}, k_{2i}, \Delta x_{c.g.}, \Delta z_{c.g.}) \right\|, \quad i = \theta, \gamma, \psi$$

The objective functions were calculated on some grid by linear interpolation of the experimental results and the results of mathematical modeling, and minimized considering $k_{1\theta}$, $k_{2\theta}$, (or $k_{1\gamma}$, $k_{2\theta}$, $k_{1\psi}$, $k_{2\psi}$), and $\Delta x_{c.g.}$, $\Delta z_{c.g.}$ as parameters. The result of the optimization for yaw channel is presented in Figure 7. In the result of minimization procedures the following parameter values were calculated:

$k_{1\theta}$=0.04, $k_{2\theta}$=0.07, $k_{1\psi}$=0.0005, $k_{2\psi}$=0.0026, $k_{1\gamma}$=0.005, $k_{2\gamma}$=0.01,$\Delta x_{c.g.}$=-0.0016(m), $\Delta z_{c.g}$ =0.0031(m).

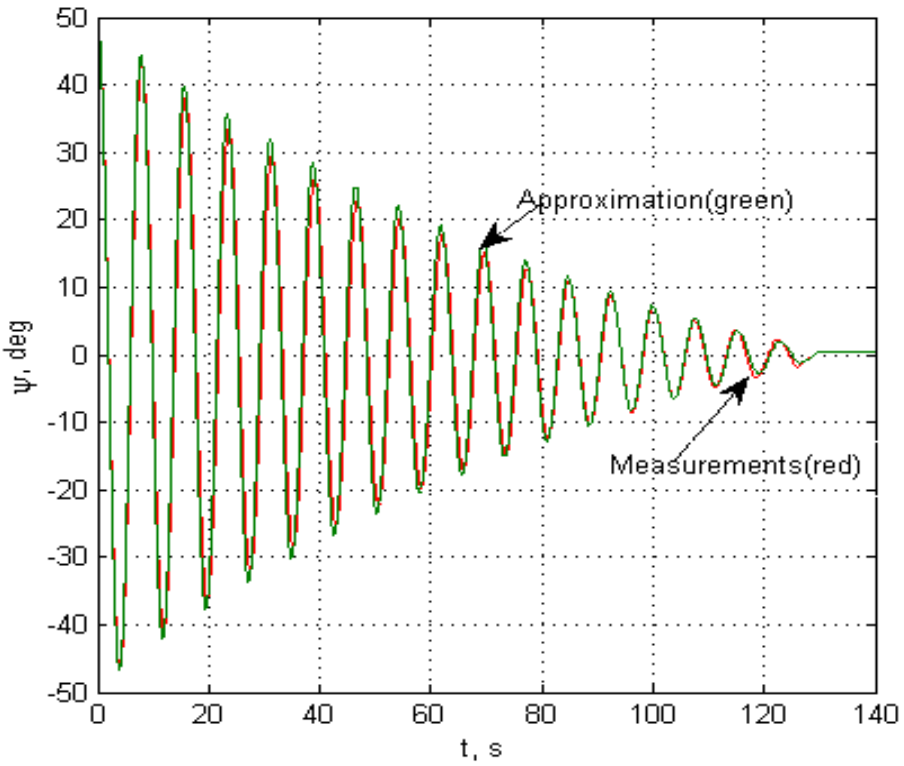

Figure 7: Fitting of experimental data: yaw oscillations in spring suspension.

Figure 8 shows an example of simulation of the perturbed model motion in the 3DOF gimbals in WT with the identified center of gravity shift and friction parameters. For comparison, dotted lines show the similar transients in the absence of friction and center of gravity shift. Flow velocity in simulation was taken equal to 25 m/s. It can be seen that influence of friction and non-ideal centers coincidence is not significant and can be neglected in many cases, in particular, for control law design.

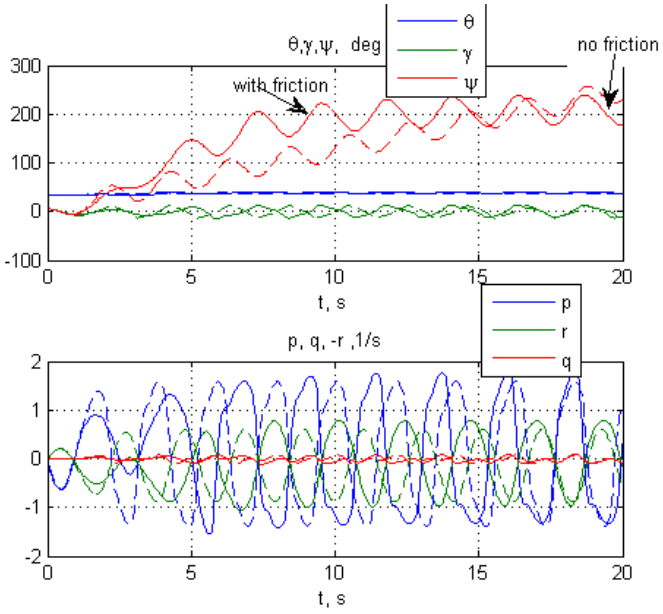

Figure 8: Simulation of self-induced oscillations of aircraft model in 3 DOF gimbal, δ_e=-23 deg.

4. Comparison of aircraft motion in 3DOF gimbals and in free flight

In order to justify the possibility of studying the dynamics of the aircraft at high angles of attack in a wind tunnel by a controlled movement of a scaled model in 3DOF gimbals, the comparison of mathematical modeling its dynamics to the mathematical modeling of the dynamics of the same model in flight is performed. In this comparison friction in gimbals and center of gravity displacement are neglected. Results of numerical simulation of wing rock motion in the 3 DOF gimbals in WT and in free flight described by the full spatial aircraft motion equations are presented in Figure 9. It can be seen that amplitudes of self-induced oscillations in angles of attack and sideslip, as well as angular rates, are rather close to each other. Oscillation frequencies are also close. Amplitudes of roll oscillation are different due to differences in equations.

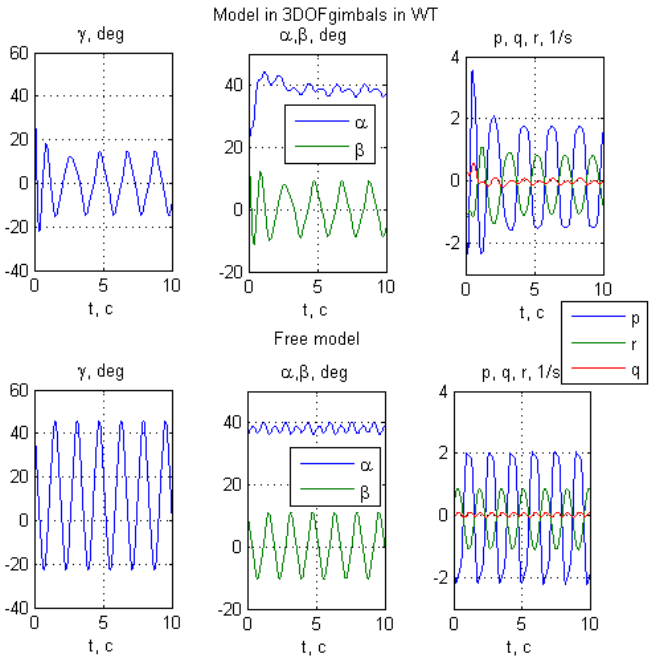

Figure 9: Comparison of wing rock oscillations in the 3 DOF gimbals in WT and in the free flight motion.

Comparison of the eigenvalues of free model motion in the vicinity of horizontal flight and in 3DOF gimbals shows that they are close to each other. For example, when $\alpha = 35^o$ eigenvalues of a short period mode of order 5 equal to 0.2282±0.5911, -0.4072±0.6654 *i*, -2.111, and for a system of order 6 in motion in 3DOF gimbal they are 0.2682±0.5687, -0.4025±0.5749 *i*, -2.187, 0, respectively. Trimmed values of elevator deflection are $\delta_{e\ trim=}$-19.741 deg., and $\delta_{e\ trim=}$-17.8947 deg., respectively. The presented comparison shows that aircraft wing rock motion can be studied using a scaled model in the 3DOF gimbals in WT.

Dependence of wing rock amplitude on elevator deflection for the considered model of maneuverable aircraft is shown in Figure 10. Periodic solutions representing the large amplitude oscillations were calculated using a technique of continuation on a parameter for an autonomous system of order 8 describing a spatial aircraft motion (in assumption of constant altitude)[18]. Here unstable equilibrium brunches of solutions are marked in blue and stable solutions are marked in red. Stable periodic solutions are shown from their minimum to maximum values marked in red (unstable branches of periodic solutions are not displayed). Wing rock exist in the interval $-28.1 < \delta_e < -22.6^o$ degrees. In both ends of this interval a complex conjugate pair of eigenvalues intersects the imaginary axis. In these points Hopf bifurcations give rise to periodic solutions. At $\delta_e = 22.6^o$ wing rock onset occurs through sub-critical bifurcation, while at $\delta_e = 28.1^o$ through a super-critical one. Inside the interval a number of periodic solution bifurcations leading chaos onset takes place. Approximate ranges of a stable chaotic attractor representing wing rock motion in the range $-26.8 < \delta_e < -25.2^o$ are also shown in Figure 10. Independently on the type of the trajectories, all these types of wing rock motion are equally dangerous, can quickly lead to stalling and they must be suppressed for a safe flight.

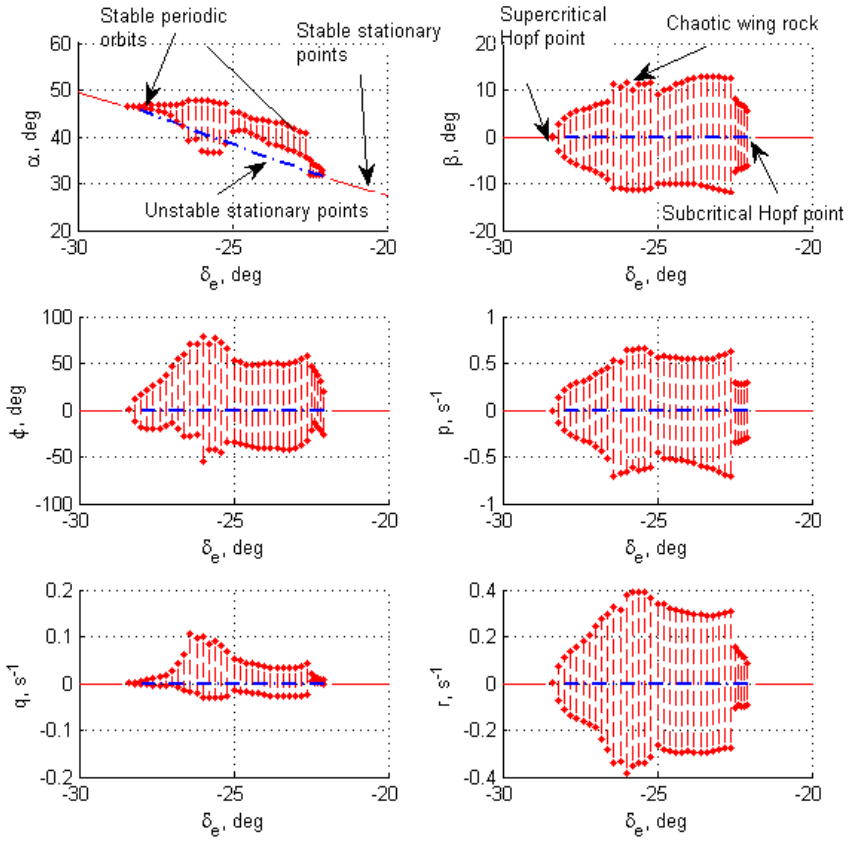

Figure 10: Level equilibrium and wing rock motion (periodic and chaotic) depending on elevator deflection.

5. Control law

The available experimental setup allows testing different control laws, which provide stability of the aircraft model in 3DOF gimbals in WT at high angles of attack, suppression of self-oscillations and prevent stalling. In this paper we propose two control laws for validation in WT. The first of these is the most simple proportional control law with

constant coefficients. It is designed using robust synthesis [16-17], the second of them is L_1 adaptive controller [19-20]. Briefly describe how they were designed.
The proportional control law for improving lateral/directional stability and suppressing wing-rock and stalling have the following form:

$$\boldsymbol{\delta}=K_\gamma\gamma+ K_\psi\psi+ K_p p+ K_r r \tag{3}$$

Where $\boldsymbol{\delta}=\Delta\delta_e$ or $\boldsymbol{\delta}=\delta_a$ or $\boldsymbol{\delta}=(\Delta\delta_e,\delta_a)$, or $\boldsymbol{\delta}=(\Delta\delta_e,\delta_r)$, that is the control effectors is differential elevator, or aileron, or two control surfaces: differential elevator with rudder or aileron. All these choices are tested because the control efficiencies of all these surfaces degrade dramatically at angles of attack higher 25^o and measured with high uncertainty. Angles γ ψ used for feedback are measured by encodes, and angular rates are measured by gyros. The control law gains were calculated using multi-model/multi-objective state-feedback synthesis with pole placement in LMI regions [16, 17]. This approach allows obtaining robust controllers for a certain range of parameters of parameter dependent plants. Given a plant with state-space equations

$$\begin{aligned}\dot{x} &= A(t)x + B_1(t)w + B_2u(t)\\ z_\infty &= C_1(t)x + D_{11}(t)w + D_{12}u(t)\\ z_2 &= C_2(t)x + D_{22}(t)u\end{aligned}$$

the method used allows to compute a state-feedback control $u = Kx$ that keeps the H_∞ norm from w to z_∞ and H_2 from w to z_2 below some prescribed values, and places the closed-loop poles in the LMI region [16].For time-varying state-space matrices ranging in the polytope

$$\begin{pmatrix} A(t) & B_1(t) & B_2(t)\\ C_1(t) & D_{11}(t) & D_{11}(t)\\ C_2(t) & 0 & D_{22}(t)\end{pmatrix} \in \mathbf{Co}\left\{\begin{pmatrix} A_k & B_{1k} & B_{2k}\\ C_{1k} & D_{11k} & D_{11k}\\ C_{2k} & 0 & D_{22k}\end{pmatrix}\right\}, k=1,\ldots K$$

the method used allows to satisfy all these requirements together.
In the present lateral/directional control law design the range of angles of attack varied from 20 up to 45^o which corresponds to trimming values of elevator deflections from -12 up to -28 degrees. The pole placement region was chosen in the intersection of the half-plane x<-1.2 and of the conic sector centered at the origin and with inner angle $3\pi/4$, and the design objective was the minimizing H_2 norm from the disturbances, including turbulence, to all the lateral/directional variables $\gamma, \psi, p, r,$ as well as control efforts (with some weights). The result of the control design procedure is the control law of the form (3). For example, for $\boldsymbol{\delta}=(\Delta\delta_e,\delta_r)$ the control law is the following:

$$\begin{bmatrix}\Delta\delta_e\\ \delta_r\end{bmatrix} = \begin{bmatrix}1.1 & -0.1 & 0.12 & 0.21\\ 1.4 & -0.8 & 0.13 & 1.2\end{bmatrix}\left[\gamma, \psi\, p, r\right]^T$$

To improve longitudinal stability and suppress pitch oscillations, a simple pitch damper is used to produce the following control input on elevator deflection $\delta_e = \delta_{e\,trim} + K_q q$ with $K_q = 0.2 \div 0.4$ .Nonlinear simulation taking into account the first order actuator model 1/(0.011s+1), time delay due to the control real-time implementation τ=0.04s, and the available aerodynamic model (2), approves the used design approach for providing lateral-directional stability. An example of the closed-loop system numerical simulation with the designed controller is shown in Figure 11. Control law is switched on at t=2s.

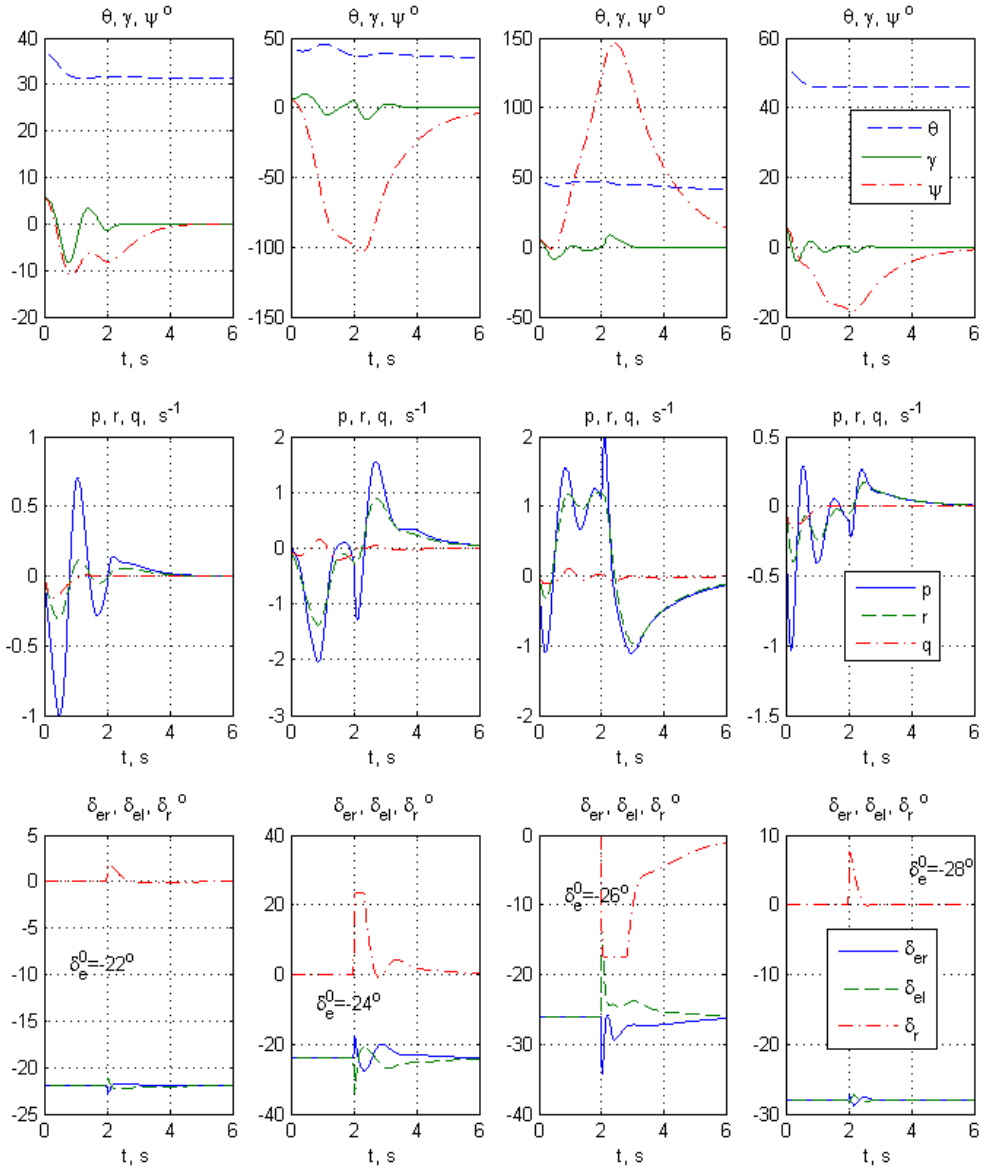

Figure 11: Wing rock developing and suppression switching on the control law at t=2s.

Attempts to design an adaptive L_1 controller [19-20] consisting on a state predictor, the adaptation law, and the control law were also performed. In the present work the two-loop configuration is implemented. The inner loop includes a simple proportional controller described before, and the outer loop is an adaptive one. The L_1 adaptive controller design method follows to [19]. An example of nonlinear simulation taking into account the actuator model, time delay due to the control implementation equal to 0.02s, and digital realization of the controller is the sampling time T_s=0.02. The simulation results presented in Figure 12 demonstrate a potential of this control law to suppress wing rock and prevent stalling

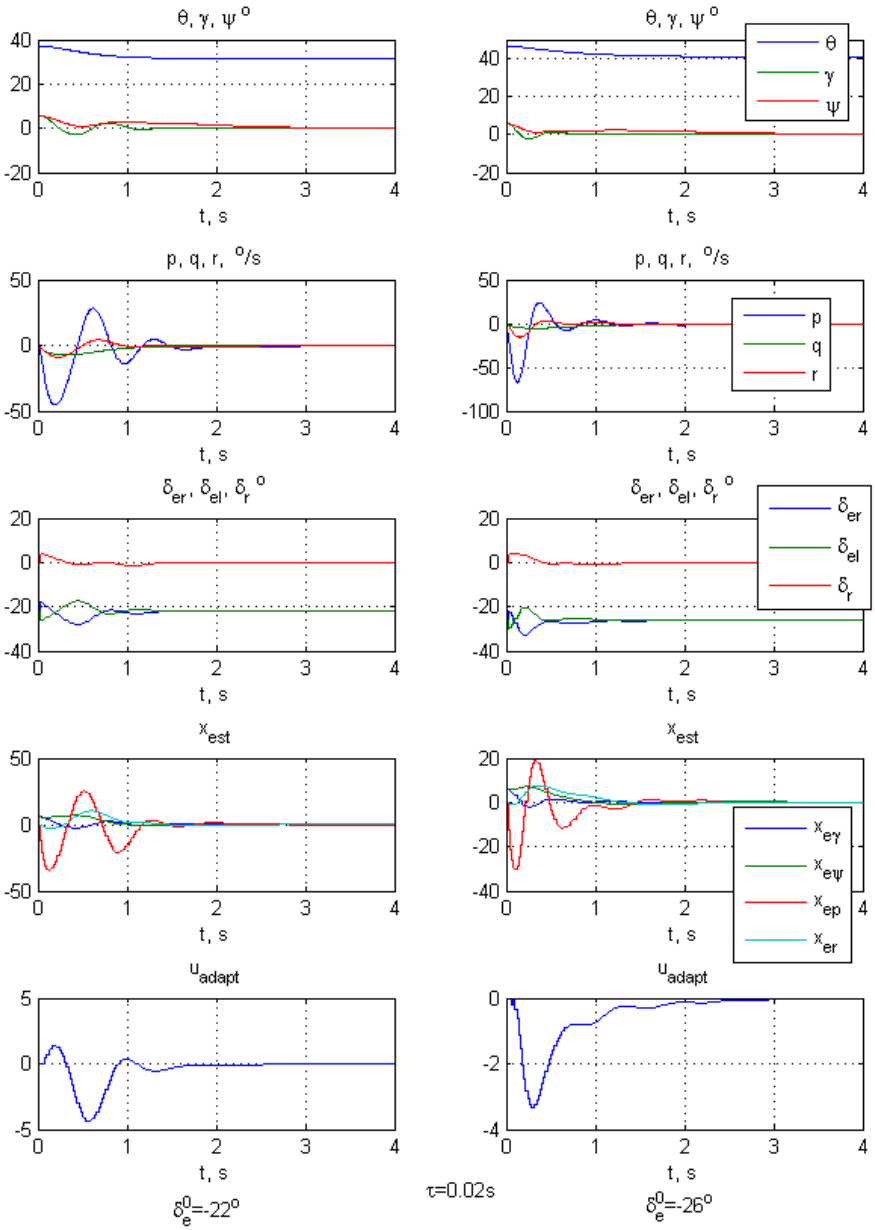

Figure 12: Wing rock suppression with adaptive controller, T_s=0.02.

5. Experimental studies

The typical open loop experimental results of the aircraft model motion in 3DOF gimbals in WT are presented in Figure 13. Measured angles, angular rates and input control surface deflection δ_{elev} (left and right) are shown. During step-wise elevator deflection the model gradually changes the trim pitch angle. The lateral stability is lost in the range $-30° < \delta_{elev} < -20°$. The model is rotating with high yawing rate. Note that in the experiment the stability is lost earlier (δ_e =-20°) than in the numerical analysis (δ_e =-22.6°). This means that it is necessary to refine the aerodynamic model. Additional experiments were executed using the same rig equipped with the internal strain-gage balance for more accurate measurements roll and yaw moments depending on angle of attack, sideslip angle and control surfaces deflections.

The records of responses in the experiment with model motion controlled by the proportional control law are shown in Figure 13. Elevator deflection is gradually increased, while the control law prevents model stalling. Residual oscillations in angle of attack and sideslip angle are about 3-5 degrees, and in roll angle are 5-8 degrees. So, the proposed control law prevents stalling and essentially suppresses wing rock.

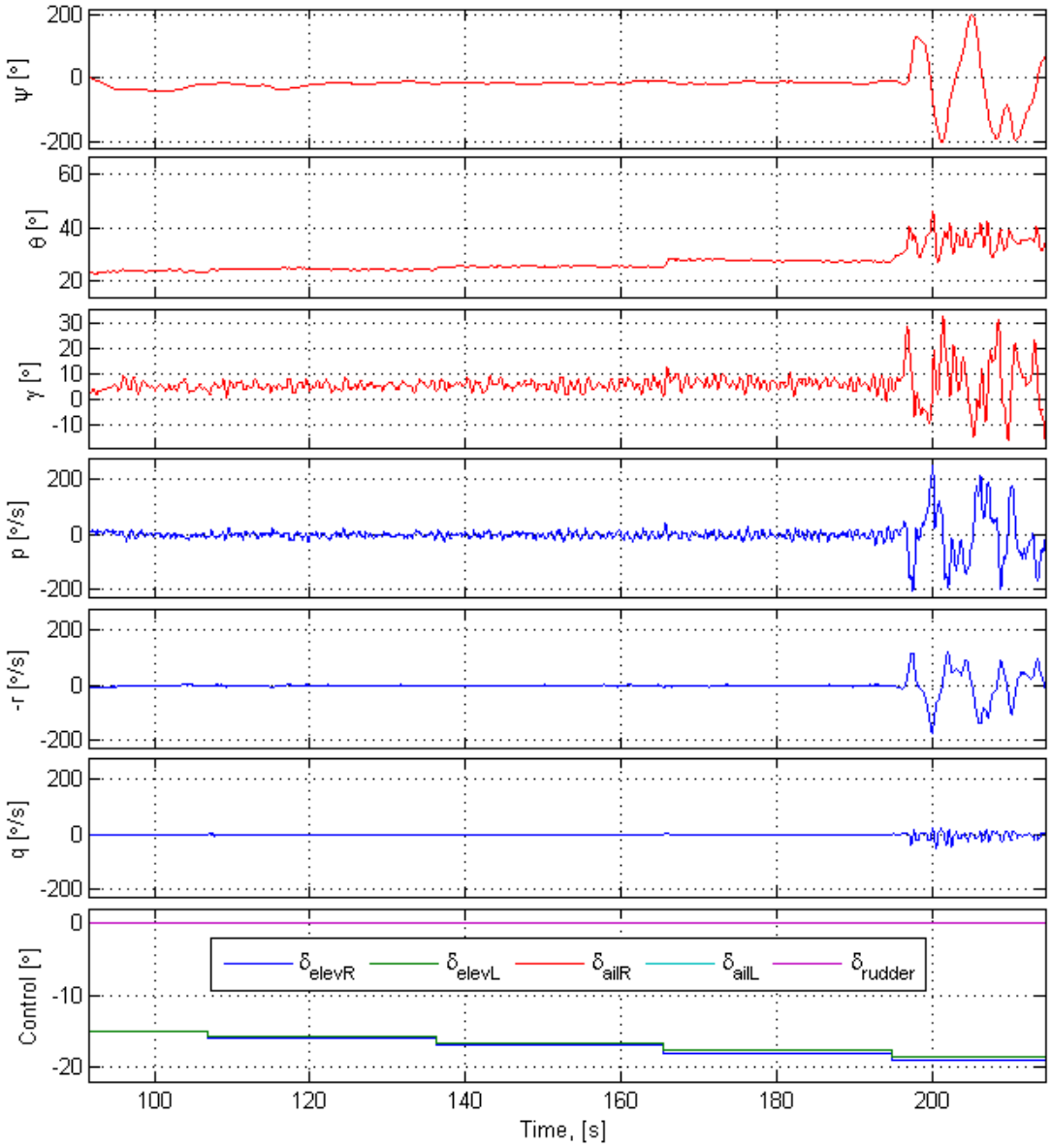

Figure 13: Open loop 3 DOF experiment

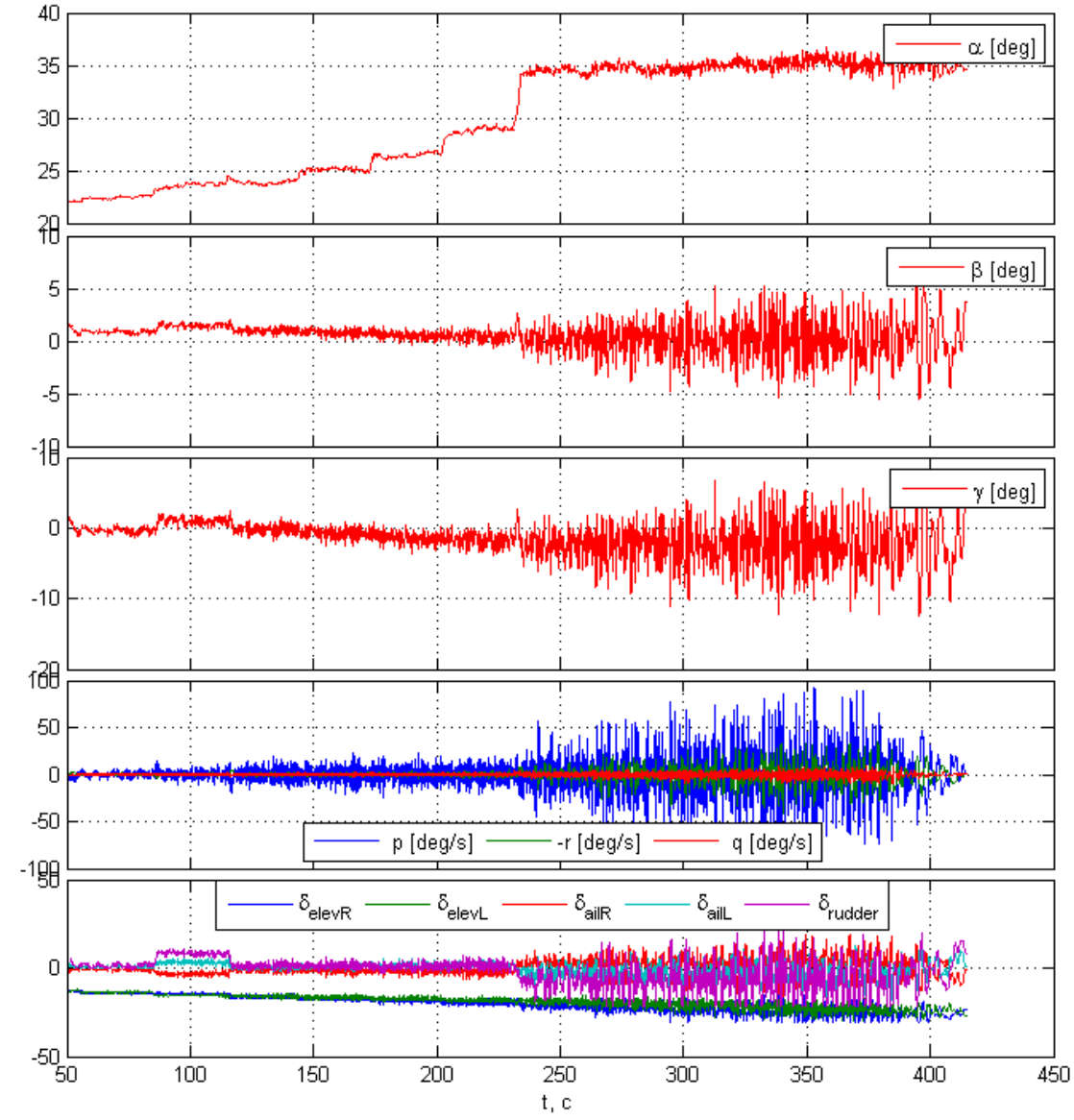

Figure 14: Closed loop 3 DOF experiment

6. Conclusions and further work

The use of an actively controlled wind tunnel model mounted on a purposely designed, three degree-of-freedom gimbals support, have shown an ability to provide investigation of critical flight regimes at high angles of attack. Friction in the gimbals has been estimated and found insignificant for high angles of attack phenomena study. Control laws for longitudinal and lateral-directional stability augmentation and stalling prevention were proposed. Experimental study of the proportional control law demonstrates promising results. Further work supposes redesign of control laws using the refined aerodynamic model and further testing of different control laws.

References

[1] Capone F.J, Owens D.B, Hall R.M. 2004. Development of a transonic free-to-roll test capability. *Journal of Aircraft*, 41.

[2] Rajamurthy M.S. 1997. Generation of comprehensive longitudinal aerodynamic data using dynamic wind tunnel simulation. *Journal of Aircraft*, 34:

[3] Bennet R.M, Farmer M.G, Mohr R.L, Hall W.E. 1978. Wind-tunnel technique for determining stability derivatives from cable-mounted models. *Journal of Aircraft*, 15:.

[4] Magill J.C, Cataldi P, Morency J.R, Hammer D.X, Anderson B.D. 2003. Design of a wire suspension system for dynamic testing in AEDC 16T. In: *41st Aerospace Science Meeting and Exhibit*,

[5] Khrabrov A, Zhuk A. 1995. Using of large amplitude free oscillations in pitch and roll to investigate unsteady aerodynamic characteristics at separated flow regimes. *ICIASF'95 Record*. - Ohio, USA, 241-247.

[6] Cook, M. V. 1987. On the use of small scale aircraft models for dynamic wind tunnel investigation of stability and control. *Trans. of the Institute of Measurement and Control*, 9: 190–197.

[7] Davison P.M, di Bernardo M., and Lowenberg M.H., 2003. Modelling and control of a single degree-of-freedom dynamic wind tunnel rig. *European Control Conference* (ECC2003), Univ. of Cambridge.

[8] Davison P, Lowenberg M.H, di Bernardo M. 2003. Experimental analysis and modeling of limit cycles in a dynamic wind-tunnel rig. *J. of Aircraft*. 40: 777-785.

[9] Papageorgiou G, Glover K. 1999. Design, development and control of the HIRM wind tunnel model. In: *European Conference on Decision and Control*.

[10] Gatto A, Lowenberg M.H. 2006. Evaluation of a three-degree-of-freedom test rig for stability derivative estimation. *J. of Aircraft*. 43: 1747-1762.

[11] Pattinson J, Lowenberg M, Goman M. 2009. A Multi-degree-of-freedom rig for the wind tunnel determination of dynamic data. In: *AIAA Atmospheric Flight Mechanics Conference*, 5727.

[12] A. Sen, N. Bhange, P. Wahi, A. Ghosh. 2009. 5-Degree-of-freedom dynamic rig for wind tunnel tests of aerospace vehicles. In: *AIAA Atmospheric Flight Mechanics Conference*, 5605.

[13] Chambers, J.R. 2009. Modeling flight: the role of dynamically scaled free-flight models in support of NASA's aerospace programs. NASA SP 575.

[14] A.N. Khrabrov, M. E. Sidoryuk, E. N. Kolesnikov, Yu. A. Vinogradov, I. I. Grishin, and K. A. Kolinko 2014. On possibility of critical flight regime study in wind tunnels using a three-degree-of-freedom gimbals, TsAGI Science Journal,. XLV: 825 — 839

[15] M. Sidoryuk, 2014. Robust control design to suppress wing rock motion of a wind-tunnel aircraft model in 3DOF gimbals, TsAGI Science Journal, XLV: 977 — 992.

[16] Chilary M., Gahinet P. 1995. H_∞ Design with pole placement constraints: an LMI approach. *IEEE Transactions on Automatic Control*. 40: .

[17] Gahinet P, Nemirovsky A, Laub A, Chilary M. *Robust control toolbox*. The Math Works Inc.

[18] Sidoryuk M. 2013. LPV control design to suppress wing rock motion. In: *5th European conference for aerospace sciences*.

[19] Kharisov E., Hovakimyan N., 2008. L1 Adaptive Control Law for Flexible Space Launch Vehicle and Proposed Plan for Flight Test Validation. In: AIAA Guidance, Navigation and Control Conference, 2008-7128.

[20] Cao C, Hovakimyan N., 2009. L1 Adaptive Output-Feedback Controller Non-Strictly-Positive-Real Reference Systems: Missile Longitudinal Autopilot Design, *J. of Guidance, Control, and Dynamics*, 32: 717-726.